www.cad-journal.net
Computer-Aided Design AND APPLICATIONS

Numerical Study of Non-Newtonian Ceramic Slurry Flow in Extrusion based Additive Manufacturing

Ishant G. Patil, Harshal Y. Shahare, Vivek V. Bhandarkar and Puneet Tandon

deLOGIC Lab, PDPM Indian Institute of Information Technology, Design and Manufacturing, Jabalpur, Madhya Pradesh – 482005, India, 20mmec04@iiitdmj.ac.in, 1823604@iiitdmj.ac.in, 1913604@iiitdmj.ac.in, ptandon@iiitdmj.ac.in

Corresponding author: Puneet Tandon, ptandon@iiitdmj.ac.in

Abstract. Extrusion-based additive manufacturing (EAM) is one of the widely used processes due to its reliability and the diversity of the material being used. The use of ceramics as a raw material is still in its nascency. Major challenges in the EAM of ceramics are the preparation of feedstock slurry and its flowability through an extruder, which plays a crucial role in the 3D printing of defect-free parts. Numerical simulation can predict the approximate outcome of complexities arising during experiments. This paper focuses on the development of a numerical model that simulates the non-Newtonian ceramic slurry flow through the nozzle of a customized cartesian 3D printer. The focus of the work lies in the implementation of the Herschel-Bulkley Papanastasiou (HBP) model for feedstock slurry to understand the behavior inside the nozzle for the uniform flow of the feedstock. A rotating viscometer is used to measure the viscosity of the slurry. The observed value is used as an input for measuring the rheological constants of the ceramic slurry. The rheological constants for the HBP model are compared with the Power-law model and Bingham plastic model to validate the best-fit model for the ceramic slurry. The variation of velocity of slurry across the length of the nozzle and surface pressure is analyzed through numerical simulation. The results are identified based on the flow behavior of ceramic slurry at different sections over the length of the extruder. The significance of inlet velocity over the printing velocity is examined. Besides, the effect of temperature on the extruder and the fluid flow is investigated with the help of numerical simulation. Further, the time-dependent study is performed to understand the effect of temperature distribution when the ceramic slurry is flowing through the extruder.

Keywords: Extrusion-based Additive Manufacturing (EAM); Ceramics; Herschel-Bulkley Papanastasiou (HBP) model; Non-Newtonian Fluid; Ceramic Slurry; Rheological Properties.
DOI: https://doi.org/10.14733/cadaps.2024.131-142

1 INTRODUCTION

Additive manufacturing (AM) is a process having a bottom-up approach where the material is added layer by layer using a defined toolpath in three dimensions with defined process parameters to obtain the final product with minimal material waste. Among all the AM processes, material extrusion (ME) is in demand due to its ability to print complex parts, low cost, and wide range of feedstock materials. Polymers are the most widely used material in EAM, while metals and ceramics are still in their initial stages of usage due to the complexity of feedstock preparation, processing difficulties, and the requirement of post-processing. Under the EAM processes, the fused filament fabrication (FFF) process uses filament feedstock loaded on a spool which is fed to the extruder and further to the nozzle, where the semi-solid material starts depositing on the build platform [15]. Moreover, direct ink writing (DIW) is another process under EAM, where the slurry or paste is used as a feedstock material and deposited using a syringe extruder or customized extruder.

Of late, the manufacturing of advanced ceramics for biomedical applications through EAM was emphasized due to their excellent properties such as high-temperature resistance and high strength [19]. Limited research has been reported on the rheological properties of non-oxide ceramic slurry flow inside the nozzle for a customized FFF process [5]. A high solid loaded slurry, i.e., solid particles comprising 50-60 wt% with the rest being water, flowing through a small diameter nozzle at a low shear rate exhibits a complex non-Newtonian flow [20]. The non-Newtonian slurry is characterized by a non-constant viscosity that differs with flow conditions [6]. The ceramic slurry shows complex rheological properties, which affect the extrudability [13]. These rheological properties of ceramic slurry can be controlled by considering several factors such as material mesh size, particle distribution, the proportion of binders, dispersants, and additives. Modeling and simulation play a vital role in understanding the complex relationship between nozzle geometry, heat transfer rates, and fluid flow, which can predict the effect on the slurry inside the nozzle [17]. Simulation of the EAM process is strenuous due to the involvement of multiphysics in various sections of modeled geometry. For non-oxide ceramic slurry in EAM, primarily experimental and analytical works have been reported, while no literature predicted the process outcome using numerical analysis. The numerical study carried out to date relies on several assumptions and model simplification to reduce the complexity and reliability of the outcome. Moreover, the previous numerical studies had been focused on the deposition rate assuming a constant velocity throughout the cross-section of defined geometry.

Previously, Golman et al. [8] worked on developing the mathematical model for the ceramic material extrusion process in the ram-type extruder. The ceramic slurry was considered a non-Newtonian Herschel-Bulkley model, while the stress growth factor was neglected. Li et al. [12] developed a similar mathematical model for ceramic slurry. The study focuses on the relationship between the plunger velocity and applied force, while the effect of heat was neglected. Lately, Xia et al. [22] demonstrated a numerical model that could predict shrinkage over time and part deformation. The paper's novelty lies in the development of the multiphysics model consisting of stress-growth factors and temperature considerations with the slurry flow.

This paper presents the numerical simulation of a non-oxide ceramic slurry flow through the nozzle of a customized FFF printer. Further, it aims to implement the Herschel-Bulkley Papanastasiou (HBP) model for the numerical study of flow analysis. The slurry is modeled as a non-Newtonian fluid where the continuity and momentum equation for the flow is solved numerically using the HBP model. The in-house developed MATLAB code is used to get the flow behavior index (n), fluid consistency coefficient (k), yield stress (σ_y), and coefficients of determination (R^2) of the slurry material. The rheological constants of the HBP model are compared with the rheological constants obtained with Power Law (PL) and Bingham Plastic (BP) models to define the nature of the slurry. The implemented model reveals the velocity and pressure profile distributions across the nozzle geometry. Further, the time-dependent study was also performed to determine the temperature distribution along the nozzle and slurry.

This paper is organized into four sections starting with an introduction and the motivation to carry out the research work. Section 2 focuses on the materials and methods used for developing customized set-up and design of slurry material. Further, it explores the computational model, assumptions, boundary conditions, and governing equations. Section 3 extends the discussions and focuses on the obtained results, while Section 4 of the manuscript presents the concluding remarks based on the observations.

2 MATERIALS AND METHODS

2.1 Customized Setup Modeling

Modeling and numerical simulation were required to upgrade the Creality Ender-3 3D printer to deposit and manufacture the ceramic parts. Autodesk Fusion 360 (Educational License) was used for the initial design of the setup. Figure 1 shows a customized 3D printer setup where the stepper motor is connected with a lead screw which is used to feed the slurry in the extruder. Figure 1 (b) shows the section view of the extruder. The extruders consist of different parts such as the throat, heating block, nozzle, heat sink, and pneumatic connector. The nozzle geometry with throat and slurry is exported to COMSOL Multiphysics. The model is designed and implemented as a 3-dimensional geometry, where the throat and nozzle are modeled as a contact assembly. The number of edges and vertices in the contact assembly are 120 and 72 respectively. The diameter at the inlet of the throat is 1.80 mm whereas, at the nozzle, it is 1.00 mm. The study is limited to the geometry of the throat and nozzle, where the cross-section varies from the inlet of the throat to the outlet of the nozzle.

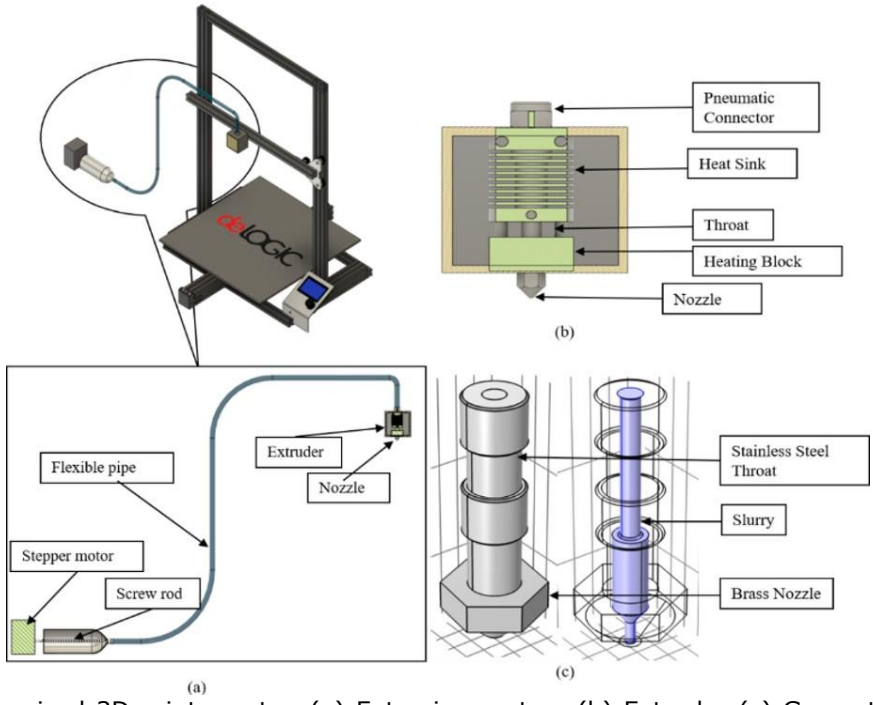

Figure 1: Customized 3D-printer setup (a) Extrusion system (b) Extruder (c) Geometry of nozzle and slurry.

2.2 Materials Properties

Boron Carbide (B_4C) ceramic of 99% purity with 220 mesh size and methylcellulose (MC) of high viscosity grade as a binder was chosen for the experimental calculations of viscosity and numerical

simulations in this work. The MC was selected as it prevents phase separation during the extrusion process and shows good flowability [4]. The experiments were conducted by preparing MC slurry, which is dispersed in the deionized water to make it 56 wt% slurry. The solid-loaded B_4C powder was mixed with the prepared slurry by using a magnetic stirrer for 2 hours at room temperature at 900 RPM. Table 1 shows the material properties of stainless steel and brass used for making the throat and nozzle respectively [7]. The ceramic slurry density was obtained using the analytical method [1].

	Stainless steel [7]	**Brass [7]**	**Slurry [1]**
Density (kg/m^3)	7,850	8,525	1,408
Thermal conductivity (W/mK)	44.5	109	30
Heat capacity (J/kgK)	475	377	1,000

Table 1: Physical and thermal properties of materials.

2.3 Computational Model

The ceramic-cellulose slurry, which passes through a small diameter of the nozzle, shows non-Newtonian behavior and shear thinning characteristics due to low shear rates [11]. Due to shear flow, the consideration of variation in viscosity is essential. Recently, the Power Law model for the tape-casting process of the ceramic slurry was investigated where constants were identified and applied to a numerical model, which influences the process of simulating ceramic slurries [10]. Power Law (PL), Bingham Plastic (BP), and the Herschel-Bulkley model can be used for ceramic slurries. Papanastasiou presented a modified Herschel-Bulkley model equation to relate strain rate tensor (D) with viscous stress tensor (τ) [16]. Due to a wide range of shear rates, the modified Herschel-Bulkley model, also known as the Herschel-Bulkley Papanastasiou (HBP) model, was implemented in this work. The HBP model describes the slurry viscosity as shown in Equation (1) [14].

$$\tau = \left(k\gamma^{n-1} + \frac{\tau_0}{\sqrt{|\Pi_D|}} \left[1 - exp\left(-m\sqrt{|\Pi_D|} \right) \right] \right) D \tag{1}$$

In the Equation (1), ($\sqrt{|\Pi_D|}$) denotes the second invariant of the strain rate tensor. τ_0, k, n, and m are yield stress, fluid consistency index, flow index, and stress growth factor respectively. The slurry shows a shear-thinning behavior when the flow index is less than 1. The shear growth parameters control the shear rate (γ). For the one-dimensional case, the HBP model, described by Equation (1) can be reduced as shown in Equation (2).

$$\tau = \left(k\gamma^{n-1} + \frac{\tau_0}{\gamma} \left[1 - exp(-m|\gamma|) \right] \right) \gamma \tag{2}$$

To determine the flow index, fluid consistency index, and yield stress, an algorithm is developed in MATLAB. Figure 2 shows the flowchart of the MATLAB code. The viscometer reading is taken as input data, which is sorted according to the developed algorithm. The measured data is then converted into shear stress and shear rate values. The updated data is plotted. Similarly, the PL, BP, and HBP models are plotted respectively. The index values are determined using the curve fitting function and performing multiple iterations. The respective parameter values for the different models are shown in Table 2. The measured data is plotted as shear stress versus shear rate, as shown in Figure 3. The coefficient of determination (R^2) for the HBP model is 99.48% while the R^2 values of the PL and BP models are 92.91% and 14.81% respectively. An R^2 value that is close to 100% is preferred. Thus, the best-fitted model is identified as the HBP model.

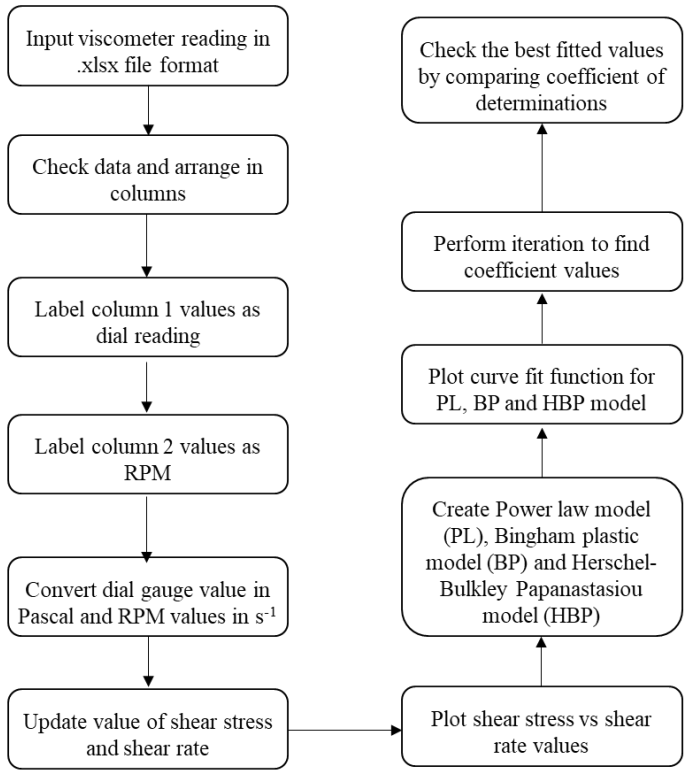

Figure 2: Flow chart to determine rheological constants and the best-fitted computational model.

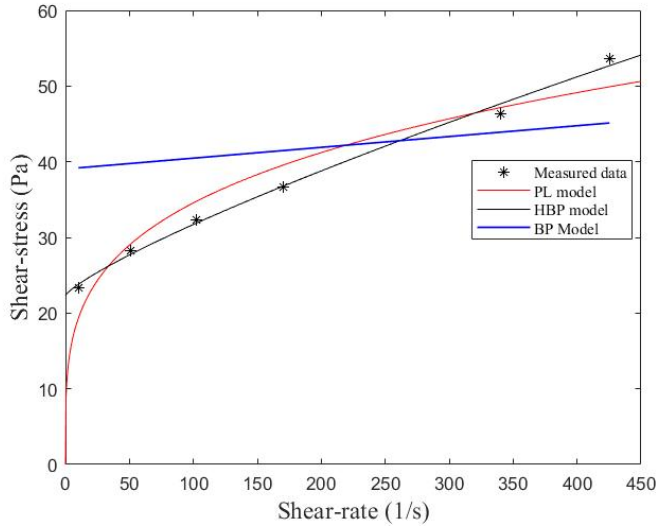

Figure 3: Comparison of different computational models to find the best-suited model.

	Power Law Model (PL)	Bingham Plastic Model (BP)	Herschel Bulkley Papanastasiou (HBP)
Flow index (n)	0.253	-	0.811
Fluid consistency index (k)	10.73	-	0.223
Plastic viscosity (PV)	-	0.142	-
Yield point (YP)	-	39.04	-
Yield stress (τ_0)	-	-	22.33
Coefficient of determination (R^2)	92.91	14.81	99.48
Stress growth factor (m)	-	-	10

Table 2: Parameters for PL, BP, and HBP models.

2.4 Assumptions and Boundary Conditions

The slurry flow from the inlet of the throat to the exit of the nozzle was assumed to be laminar. The throat and nozzle were filled with the slurry without any void formation, and it was considered an incompressible flow. The slurry does not experience the slip at the wall of the nozzle. The ambient temperature was considered at the inlet of the throat as well as at the outlet of the nozzle. A time-dependent study was performed to understand heat transfer in solid and fluid, while a stationary study was performed to understand the slurry flow behavior. The heat flux and heat rate were considered 30 W/m^2 and 40 W respectively. To simulate the temperature-controlled heating of the liquefier, a constant temperature was considered, which is equal to the extrusion temperature.

2.5 Governing Equations

For the ceramic slurry flow profile inside the throat and nozzle geometry, the continuity equation and momentum equation are given by Equation (3) and Equation (4) respectively, which are simultaneously solved through iterations [2].

$$\frac{\partial \rho}{\partial t} + \nabla.(\rho u) = 0 \tag{3}$$

$$\rho \frac{\partial u}{\partial t} + \rho(u.\nabla)u = \nabla.[-pI + \tau] + F + \rho g \tag{4}$$

Where u refers to the velocity of slurry flow, ρ is the density of slurry material, p is pressure, τ is the viscous stress tensor, F is the force vector, and g is the gravitational constant. Equation (4) describes the viscous flow in a laminar state, which is also applicable to weakly compressible flows. The temperature profile across the slurry geometry and solid can be achieved by solving Equation (5) and Equation (6) [3].

$$\rho C_p \frac{\partial T}{\partial t} + \rho C_p u.\nabla T + \nabla.q = Q \tag{5}$$

$$q = -k\nabla T \tag{6}$$

Where, C_p is the heat capacity at constant pressure, Q is a heat source, k is the thermal conductivity of the slurry, ∇T is a temperature gradient, and q refers to the heat flux. In addition, to perform the numerical simulation of slurry flow where the slurry properties are dependent on the temperature, non-isothermal flow multiphysics coupling needs to be solved by using Equation (7). In the non-isothermal flow equation, operator ":" refers to the contraction between the viscous stress and velocity gradient.

$$Q = \tau : \nabla u \tag{7}$$

3 RESULTS AND DISCUSSION

This section presents the results and discussion based on the numerical simulation of ceramic slurry inside the throat and nozzle. For velocity and surface pressure distribution on slurry, Equation (3) and Equation (4) were used where properties such as slurry density, initial velocity, viscous stress tensor and pressure were considered. Similarly, Equation (5) and Equation (6) are used for the temperature distribution profile where a heat source, heat capacity, heat flux, temperature gradient and thermal gradient were considered.

3.1 Velocity and Surface Pressure Distribution on Slurry Inside the Throat Nozzle

A time-independent study was performed to understand the applied HBP model for the slurry flow simulation. Figure 4 shows the velocity variation of the ceramic slurry across the length of the throat and nozzle at a temperature of 220°C. The laminar flow and heat transfer modules are coupled to calculate the exit velocity through the nozzle and velocity variation across the length at the non-constant temperature. The inlet velocity is taken as 5 mm/s such that the lead screw moves the slurry to the extruder. The inlet velocity is completely dependent on the rotations of the lead screw, which is controlled by the stepper motor. Due to the non-isothermal flow, the viscosity of the slurry changes, which significantly impacts the flow behavior. To understand the flow behavior, the nozzle throat geometry is divided into 3 sections according to the change in the cross-section area as shown in Figure 4.

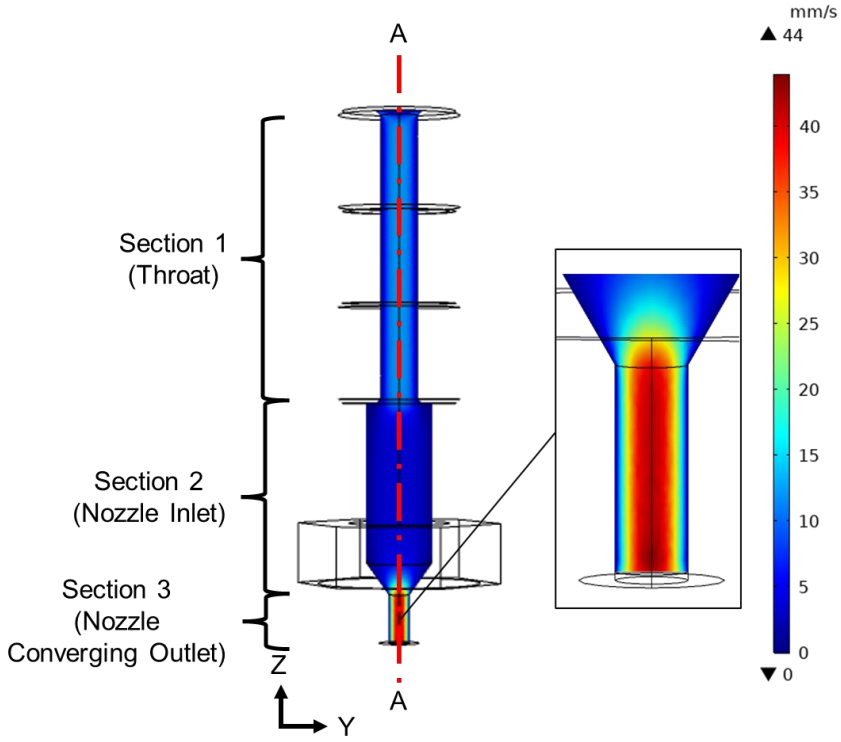

Figure 4: Variation of velocity across the length of the nozzle.

The velocity is constant and uniform across the throat region, while the velocity increases significantly across the conical region due to a decrease in the cross-section area. The maximum

exit velocity of 44 mm/s is achieved due to 56 wt% solid loading in the slurry. To increase the exit velocity, the content of solid particles should be low. Figure 55 shows the velocity variation of ceramic-cellulose slurry, where the velocity distribution is measured along the AA plane. The velocity distribution in Section 1 shows the velocity from the throat inlet to the throat outlet, which is uniform throughout the length of the throat, while it decreases across the Y-direction due to the boundary layer principle. Section 2 shows a sudden decrease in the velocity along the length due to a sudden increase in the cross-section area, while the velocity across the Y-direction remains uniform throughout the section. The sudden increase of velocity at the end of section 2 is due to the convergence of the cross-section area along the length. Section 3 shows a sudden increase in velocity from 17 mm/s to 44 mm/s due to the reduction of the cross-section area. The narrow part of the nozzle leads to higher shear stress, affecting the velocity near the wall.

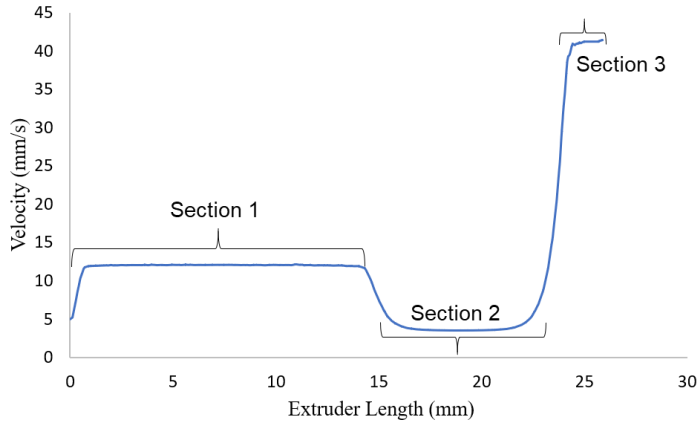

Figure 5: Velocity variation of ceramic-cellulose slurry in Section 1 (throat), Section 2 (nozzle inlet), and Section 3 (nozzle converging outlet).

The surface pressure distribution across the length of the slurry due to the solid-fluid interaction is demonstrated in Figure 6. Force acting on the slurry due to the change in cross-sections contributes to the surface pressure. The maximum surface pressure is found at the inlet of the throat. The surface pressure drops as it approaches the nozzle outlet as the forces applied by the wall of varying conical sections over the slurry decompose into radial and transverse components.

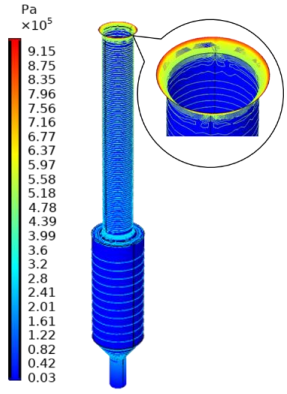

Figure 6: Surface pressure on slurry throughout the length of throat nozzle assembly.

Due to the typical shear thinning behavior, the ceramic slurry is considered extrudable when the applied force is greater than the yield stress of the slurry. Figure 77 represents the ceramic slurry viscosity flow curves at varying shear rates. Initially, the random collisions among the particles of ceramic-cellulose naturally resist the flow in a near-equilibrium slurry, resulting in high viscosity in the lower shear rates. However, with an increase in shear rate, the ceramic-cellulose particles organized and settled in a streamlined flow, resulting in a decrease in viscosity [9],[18],[21].

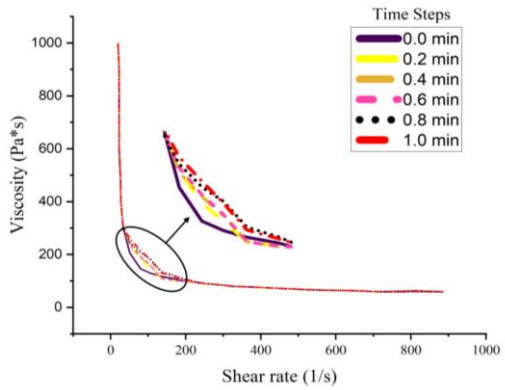

Figure 7: Ceramic slurry viscosity vs shear rate plot at varying shear rates at different simulated times.

3.2 Temperature Distribution on the Slurry and the Throat Nozzle

A fluctuation can generate clogging in the nozzle thus a constant temperature of 220 °C is applied to the liquefier. The temperature over the nozzle region is achieved through heat conduction. Figure 8 shows a temperature distribution near the wall of the nozzle from where the heat is conducted. Initially, the throat and nozzle are in ambient condition. Figure 8 (b) shows a non-uniform temperature distribution across the length after 0.6 minutes. This non-uniform temperature distribution over the length of the throat nozzle affects the viscosity which directly affects the slurry flow behavior. As the heat transfer from the throat to the surrounding is forced convection, this leads to a decrease in the temperature affecting the flowability in the nozzle. High temperature in the nozzle leads to a good flowability of the ceramic slurry. Figure 9 demonstrates the time-dependent temperature profile along the length of the throat nozzle geometry, where the temperature distribution is obtained from the non-isothermal model. The maximum temperature at the upper part of the throat reached up to 230 °C.

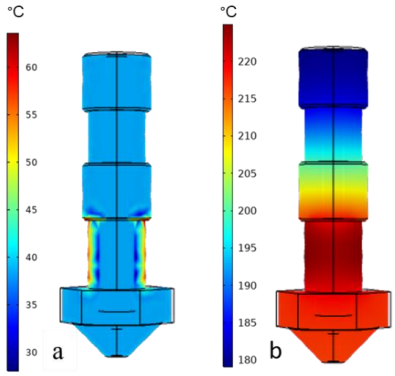

Figure 8: Temperature distribution at (a) simulation time = 0 min (b) simulation time = 0.6 min.

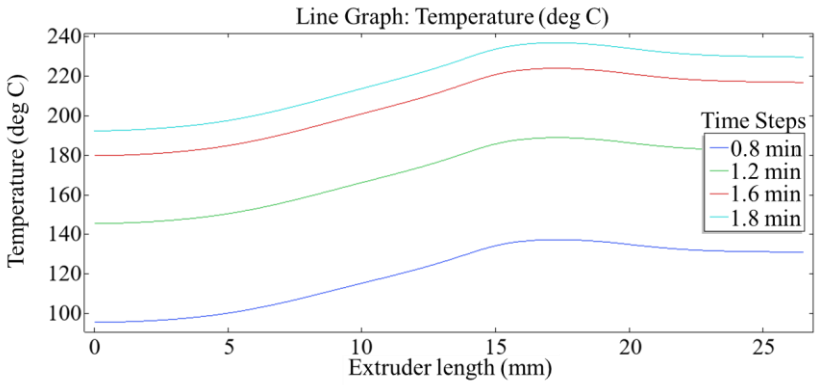

Figure 9: Time-dependent temperature distribution along the length of throat nozzle assembly.

It is crucial in many industrial operations to accurately predict the flow behavior of non-Newtonian fluids, typically those involving complex materials such as ceramics. Upon analyzing the simulation results, it was observed that the input pressure influenced the exit velocity of the slurry more than the temperature. The effect of a change in cross-section on the surface pressure of the slurry was found to be significant, suggesting that the extruder geometry could have a substantial impact on the flow behavior of the slurry. In addition, it was observed that an increase in temperature resulted in better flowability of the slurry. These findings show that the slurry temperature influences the flow of slurry significantly, which has significant ramifications for industrial processes. The experimental validation of various non-Newtonian slurry is essential to ensure reliable simulation results and validate the numerical model. Furthermore, the insights gained from this study could be used to optimize the design of extruders for processing non-Newtonian slurries, to improvise efficiency and cost-effectiveness.

4 CONCLUSION

This work investigates the numerical model to simulate non-Newtonian ceramic slurry in the EAM process. The computational model is established to find the rheological constants of HBP models. The continuity and momentum equations of the slurry are solved based on the developed HBP model. The HBP numerical model predicts the velocity distribution from the throat inlet to the nozzle outlet. The exit velocity of the slurry is more influenced by input pressure rather than the temperature due to the content of solid ceramic particles in the slurry and the higher melting temperature of the ceramic material. The effect of change in the cross-section area in geometry shows significant effects on the surface pressure of the slurry. Further, the higher temperature at the throat achieves better flowability due to the melting of the binder material of the slurry.

Ishant G. Patil, https://orcid.org/0000-0003-3627-6001
Harshal Y. Shahare, https://orcid.org/0000-0002-4897-802X
Vivek V. Bhandarkar, https://orcid.org/0000-0003-2213-6534
Puneet Tandon, https://orcid.org/0000-0001-7146-023X

REFERENCES

[1] Baha Abulnaga, P.: Slurry systems handbook, McGraw-Hill Education, 2021.
[2] Balani, S. B.; Chabert, F.; Nassiet, V.; Cantarel, A.: Influence of printing parameters on the stability of deposited beads in fused filament fabrication of poly (lactic) acid, Additive Manufacturing, 25, 2019, 112-121. https://doi.org/10.1016/j.addma.2018.10.012
[3] Behdani, B.; Senter, M.; Mason, L.; Leu, M.; Park, J.: Numerical study on the temperature-dependent viscosity effect on the strand shape in extrusion-based additive manufacturing,

Journal of Manufacturing and Materials Processing, 4(2), 2020, 46. https://doi.org/10.3390/jmmp4020046

[4] Cai, K.; Román-Manso, B.; Smay, J. E.; Zhou, J.; Osendi, M. I.; Belmonte, M.; Miranzo, P.: Geometrically complex silicon carbide structures fabricated by robocasting, Journal of the American Ceramic Society, 95(8), 2012, 2660-2666. https://doi.org/10.1111/j.1551-2916.2012.05276.x

[5] Chen, Z.; Li, Z.; Li, J.; Liu, C.; Lao, C.; Fu, Y.; Liu, C.; Li, Y.; Wang, P.; He, Y.: 3D printing of ceramics: A review, Journal of the European Ceramic Society, 39(4), 2019, 661-687. https://doi.org/10.1016/j.jeurceramsoc.2018.11.013

[6] Comminal, R.; Hattel, J. H.; Spangenberg, J.: Numerical simulations of planar extrusion and fused filament fabrication of non-Newtonian fluids, Annu. Trans. Nord. Rheol. Soc, 25, 2017, 263-270.

[7] Dayam, S.; Priyadarshi, S.; Tandon, P.: Simulation of Extrusion of Thermoplastic Binder in Additive Manufacturing Process, Advances in Additive Manufacturing and Joining, Springer, 2020, 319-328. https://doi.org/10.1007/978-981-32-9433-2_28

[8] Golman, B.; Piotr S.; Wittaya, J: Modeling and Numerical Study of Ceramic Paste Extrusion, MATEC Web of Conferences, 2021, 02011. https://doi.org/10.1051/matecconf/202133302011

[9] Huang, T.; Mason, M. S.; Hilmas, G. E.; Leu, M. C.; Freeze-form extrusion fabrication of ceramic parts, Virtual and Physical Prototyping, 1(2), 2006, 93-100. https://doi.org/10.1080/17452750600649609

[10] Jabbari, M.; Bulatova, R.; Hattel, J. H.; Bahl, C. R.: An evaluation of interface capturing methods in a VOF based model for multiphase flow of a non-Newtonian ceramic in tape casting, Applied Mathematical Modelling, 38(13), 2014, 3222-3232. https://doi.org/10.1016/j.apm.2013.11.046

[11] Ji, H.; Zhang, X.; Huang, X.; Zheng, L.; Ye, X.; Li, Y.; Effect of extrusion on viscoelastic slurry 3D print quality: numerical analysis and experiment validation, SN Applied Sciences, 1(9), 2019, 1-11. https://doi.org/10.1007/s42452-019-1097-9

[12] Li, M.; Tang, L.; Xue F.; Landers, R.: Numerical simulation of ram extrusion process for ceramic materials, Proc. 22nd Annual International Solid Freeform Fabrication Symposium, Austin, TX, 2011, 290-308.

[13] Liu, H. J.; Li, Y. M.; Li, D. J.: Research on rheological properties and extrusion behavior of aqueous alumina paste in paste-extrusion-based SFF processes, International Journal of Advanced Manufacturing Technology, 83(9-12), 2016, 2039-2047. https://doi.org/10.1007/s00170-015-7720-z

[14] Mishra, K.; Grob, L.; Kohler, L.; Zimmermann, S.; Gstöhl, S.; Fischer, P.; Windhab, E. J.: Entrance flow of unfoamed and foamed Herschel–Bulkley fluids, Journal of Rheology, 65(6), 2021, 1155-1168. https://doi.org/10.1122/8.0000286

[15] Özden, I.; Iveković, A.; Kocjan, A.: Additive Manufacturing of Ceramics from Thermoplastic Feedstocks, Open Ceramics, 6, 2021, 100129. https://doi.org/10.1016/j.oceram.2021.100129

[16] Papanastasiou, T. C.: Flows of materials with yield, Journal of rheology, 31(5), 1987, 385-404. https://doi.org/10.1122/1.549926

[17] Patel, M. J.; Blackburn, S.; Wilson, D. I.: Modelling of paste ram extrusion subject to liquid phase migration and wall friction, Chemical Engineering Science, 172, 2017, 487-502. https://doi.org/10.1016/j.ces.2017.07.001

[18] Peng, E.; Zhang, D.; Ding, J.: Ceramic robocasting: recent achievements, potential, and future developments, Advanced Materials, 30(47), 2018, 1802404. https://doi.org/10.1002/adma.201802404

[19] Rane, K.; Strano, M.: A comprehensive review of extrusion-based additive manufacturing processes for rapid production of metallic and ceramic parts, Advances in Manufacturing, 7(2), 2019, 155-173. https://doi.org/10.1007/s40436-019-00253-6

[20] Shahzad, A.; Lazoglu, I.: Direct ink writing (DIW) of structural and functional ceramics: Recent achievements and future challenges, Composites Part B: Engineering, 225, 2021, 109249. https://doi.org/10.1016/j.compositesb.2021.109249

[21] Stuecker, J. N.; Cesarano Iii, J.; Hirschfeld, D. A.: Control of the viscous behavior of highly concentrated mullite suspensions for robocasting, Journal of Materials Processing Technology, 142(2), 2003, 318-325. https://doi.org/10.1016/S0924-0136(03)00586-7

[22] Xia, H.; Lu, J.; Tryggvason, G.: Fully resolved numerical simulations of fused deposition modeling. Part II–solidification, residual stresses, and modeling of the nozzle, Rapid Prototyping Journal, 2018, 24(6) 973-987. https://doi.org/10.1108/RPJ-11-2017-0233